

Contents lists available at ScienceDirect

### Journal of Energy Chemistry



http://www.journals.elsevier.com/

journal homepage: www.elsevier.com/locate/jechem

## Computational screening for novel solid-state electrolytes in Li<sub>3</sub>MX<sub>6</sub> composition

Olgert L. Dallakyan <sup>a,b</sup>, Alexey P. Maltsev <sup>c</sup>, Ilya V. Chepkasov <sup>c</sup>, Misha A. Aghamalyan <sup>d</sup>, Areg A. Hunanyan <sup>d</sup>, Nane Z. Petrosyan <sup>d</sup>, Mikayel S. Chobanyan <sup>d</sup>, Mikayel T. Sahakyan <sup>d</sup>, Luiza G. Khachatryan <sup>d</sup>, Artem R. Oganov <sup>c</sup>, Hayk A. Zakaryan <sup>d,\*</sup>

#### ARTICLE INFO

# Article history: Received 9 July 2025 Revised 21 August 2025 Accepted 21 August 2025 Available online 2 September 2025

Keywords: Solid state electrolyte Halides Novel materials

#### ABSTRACT

Halide solid-state electrolytes have gained significant attention in recent years due to their high ionic conductivity, making them promising candidates for future all-solid-state batteries. Recent studies have identified numerous crystal structures with the  ${\rm Li_3MX_6}$  composition, although many remain unexplored across various chemical systems. In this research, we developed a comprehensive method to examine all conceivable space groups and structures within the  ${\rm Li-M-X}$  system, where M includes In,  ${\rm Ga}$ , and La, and X includes F, Cl, Br, and I. Our findings revealed two metastable structures:  ${\rm Li_3InF_6}$  with  ${\rm P3\,c1}$  symmetry and  ${\rm Li_3InI_6}$  with  ${\rm C2/c}$  symmetry, exhibiting ionic conductivities of 0.55 and 2.18 mS/cm at 300 K, respectively. Notably, the trigonal symmetry of  ${\rm Li_3InF_6}$  demonstrates that high ionic conductivities are not limited to monoclinic structures but can also be achieved with trigonal symmetries. The electrochemical stability windows, mechanical properties, and reaction energies of these materials with known cathodes suggest their potential for use in all-solid-state batteries. Additionally, we predicted the stability of novel materials, including  ${\rm Li_5InCI_8}$ ,  ${\rm Li_5InBr_8}$ ,  ${\rm Li_5InI_8}$ ,  ${\rm LiIn_2CI_9}$ ,  ${\rm LiIn_2Br_9}$ , and  ${\rm LiIn_2I_9}$ .

© 2025 Science Press and Dalian Institute of Chemical Physics, Chinese Academy of Sciences. Published by Elsevier B.V. and Science Press. All rights are reserved, including those for text and data mining, Al training, and similar technologies.

#### 1. Introduction

The demand for energy storage solutions, particularly batteries, is experiencing exponential growth and is projected to reach unprecedented levels by 2030, surpassing the capabilities of current technologies [1]. Among the emerging technologies, all-solid-state lithium-ion batteries (ASSBs) utilizing solid electrolytes stand out as promising candidates [2]. These batteries offer notable safety and energy density advantages, albeit facing challenges such as interface stability with electrodes and low ionic conductivity [3]. For example, sulfides such  $\text{Li}_{10}\text{GeP}_2\text{S}_{12}$  and  $\text{Li}_7\text{P}_3\text{S}_{11}$  have high ionic conductivity (about 1 mS/cm) but lack stability against electrodes [4]. Oxides such as  $\text{Li}_6\text{PO}_5\text{Cl}$  have low conductivity but are stable against electrodes and moisture [2]. Consequently, extensive

E-mail address: hayk.zakaryan@ysu.am (H.A. Zakaryan).

research efforts are underway to discover novel solid-state electrolyte (SSE) materials capable of addressing these limitations [4]. Despite sulfides and oxides, halides emerge as promising candidates for solid-state electrolytes which can meet all requirements for SSE [5]. Early investigations into their ionic conductivity dating back to 1930 [6], a significant breakthrough occurred only in 2018 [7], by Asano et al. Their groundbreaking work unveiled the experimental synthesis of Li<sub>3</sub>YCl<sub>6</sub> (isostructural to Li<sub>3</sub>ErCl<sub>6</sub> with the P3 m1 space group) and Li<sub>3</sub>YBr<sub>6</sub> (isostructural to  $Li_3ErBr_6$  with the C2/m space group), having impressive ionic conductivities of 0.51 and 1.71 mS/cm, respectively [7]. The fact that Li<sub>3</sub>YCl<sub>6</sub> and Li<sub>3</sub>YBr<sub>6</sub> have high ionic conductivity along with hexagonal close-packed (hcp) and cubic close-packed (ccp) anion sub-lattices respectively, attracted much interest to Li<sub>3</sub>MX<sub>6</sub> materials [3]. This structural insight has induced a wave of research aimed at identifying novel Li<sub>3</sub>MX<sub>6</sub> SSE candidates (where M encompasses elements from groups 3 and 13 of the periodic table,

<sup>&</sup>lt;sup>a</sup> Asymmetric Catalysis Research Group, Yerevan State University, Alex Manoogian 1, Yerevan 0025, Armenia

<sup>&</sup>lt;sup>b</sup> Liquid Crystalline Nanosystems Laboratory, A.B. Nalbandyan Institute of Chemical Physics NAS RA, Yerevan, Armenia

<sup>&</sup>lt;sup>c</sup> Skolkovo Institute of Science and Technology, Bolshoy Boulevard 30, bld. 1, Moscow 121205, Russia

<sup>&</sup>lt;sup>d</sup> Computational Materials Science Laboratory, Yerevan State University, Alex Manoogian 1, Yerevan 0025, Armenia

<sup>\*</sup> Corresponding author.

such as In, Ga, La, Yb, and others, and X denotes F, Cl, Br, or I), leveraging these findings as a guiding design principle [8-10]. For instance, Li et al. demonstrated the stability and high ionic conductivity of  $Li_3InCl_6$  with C2/m symmetry group, achieving a conductivity of 1.49 mS/cm alongside excellent air and water stability [11]. Similarly, Li<sub>3</sub>InBr<sub>6</sub>, possessing the same symmetry group [12], exhibited a conductivity of approximately 1 mS/cm [8]. The intricate mechanism of ion migration within these materials was elucidated in detail by Wang et al. through ab initio molecular dynamics (AIMD). In both Li<sub>3</sub>YCl<sub>6</sub> and Li<sub>3</sub>YBr<sub>6</sub>, characterized by hexagonal (hcp) and cubic (ccp) close-packed anion motifs, respectively, ion diffusion occurs via Li-ion hopping between octahedral sites through existing vacant sites with minimal energy barriers [13]. Notably, ccp Li<sub>3</sub>YBr<sub>6</sub> demonstrates isotropic fast Li<sup>+</sup> diffusion, while hcp Li<sub>3</sub>YCl<sub>6</sub> exhibits anisotropic diffusion, featuring fast onedimensional c-channels, albeit vulnerable to blocking defects such as Y – Li anti-sites [13]. Given the three-dimensional nature of Liion migration paths and the low activation barriers associated with ccp frameworks (monoclinic crystal structure), some researchers propose these structures as promising candidates for solid-state electrolytes [9,13,14].

In several studies [9,15], researchers have explored the relationship between the crystal symmetry types of halides and their implications for the design of solid-state electrolytes (SSEs). Depending on cation ordering and structural distortion, crystals featuring hexagonal close-packed (hcp) and cubic close-packed (ccp) anion sublattices can exhibit various symmetries. For the hcp anion sublattice, two distinct crystal structures have been identified: the trigonal structure observed in Li<sub>3</sub>ErCl<sub>6</sub> (space group P3m1) and the orthorhombic structure seen in Li<sub>3</sub>YCl<sub>6</sub> (space group Pnma) [15]. On the other hand, the ccp anion sublattice can give rise to structures such as the disordered spinel Li<sub>2</sub>Sc<sub>2</sub>/<sub>3</sub>Cl<sub>6</sub> (space group Fd 3 m) and the monoclinic Li<sub>3</sub>ErCl<sub>6</sub> (space group C2/m) [13]. While chloride compounds Li<sub>3</sub>MCl<sub>6</sub> can adopt either hcp or ccp anion sublattices (with M including Er, Y, Yb, among others), all known bromide counterparts Li<sub>3</sub>MBr<sub>6</sub> (with M ranging from Y to Lu) exhibit a monoclinic structure with ccp anion sublattice (space group C2/m). Wang et al. suggested prioritizing the design of chloride and bromide SSEs due to their wider electrochemical stability window compared to oxides, iodides, and sulfides, along with their relatively high ionic conductivity [13]. While many investigations concentrate on the symmetry (trigonal, orthorhombic, and monoclinic) of halides, some researchers have explored other symmetries or space groups. For instance, Park et al. used a data-mined structure predictor (DMSP) and identified the most common space groups within Li<sub>3</sub>MCl<sub>6</sub> as C2 (monoclinic), P321 (trigonal), and Pna2<sub>1</sub> (orthorhombic) [16]. In another study, Xu et al. computationally predicted novel metastable Li<sub>3</sub>LaI<sub>6</sub> and stable Li<sub>3</sub>ScI<sub>6</sub> structures with the C2 space group, which exhibit high ionic conductivity [17]. These investigations demonstrate that the possible structures of halide SSEs are not confined to trigonal symmetry, particularly the P3m1 space group, and monoclinic symmetry, particularly the C2/m space group. A more comprehensive investigation is necessary to search for novel structures within other crystal symmetries. For example, in systems like Li - In - I, Li - La - Cl, Li - Ga - Cl, and many others, the  $Li_3MX_6$  composition in the C2/m space group and monoclinic symmetry has not been identified either experimentally or computationally.

In this study, we undertake a detailed examination of all conceivable space groups and structures within the Li-M-X system (M=In,Ga, and La, and X=F,Cl,Br, and I), leveraging open databases such as Materials Project [18], OQMD [19] and literature sources not included in these databases or not predicted by DMSP or DeepMind [17,20–23]. Our objective is to discover novel solid-state electrolyte materials with the  $\text{Li}_3\text{MX}_6$  composition.

#### 2. Methods

Several effective methods are available for conducting structure searches. For instance, the utilization of evolutionary algorithms integrated into USPEX [24–27] has proven successful in predicting novel materials within the Li-Ge system [28], showcasing high ionic conductivity and introducing a new class of Ca-ion anode materials [29]. Additionally, the DeepMind team recently employed artificial intelligence to predict approximately 421,000 novel structures [20], demonstrating the potential of AI, which included new symmetry-aware partial substitutions (SAPS) [30] and random structure search combined with graph neural networks (GNNs) for stability calculation [20]. While these methods excel at uncovering previously unknown structures, they come with a significant computational cost during training step in creating DeepMind database or energy minimization step with ab initio methods in USPEX [31–38].

The simplest approach to structure prediction is the substitution of one atom type with a chemically similar atom in a known structure, followed by the calculation of stability using a convex hull diagram. This method forms the basis of the Data Mined Structure Prediction (DMSP) tool [39]. In previous studies, DMSP method has been applied to explore novel stable solid-state electrolytes within the Li-In-Cl system [16]. The method calculates the probability of stability after substitution using a probabilistic method trained on an experimental database of crystal structures [18,39]. However, it is important to note that the stability of predicted structures must be verified through density functional theory (DFT) calculations [40,41].

In our research, the detailed structure examination and novel material search were conducted in five steps, as illustrated in Fig. 1. First, we collected a comprehensive structure database consisted from 3 parts, which are (a) novel materials from DeepMind, comprising over 400,000 structures, (b) structures generated by DMSP for M = In, Ga, La and (c) structures gathered from literature that were not included in the previous datasets. Second, we performed filtration of the structures. For the DeepMind database, we selected halide ternary structures with M = In, Ga, La. The filtration step for the DMSP method was performed using Li - M - X as input systems. Structures from the literature that were not included in DeepMind and were not predicted by DMSP were added in the final part of the filtration step. Third, after the filtration step, all gathered structure types were used for substitution, replacing Na with Li, metals with Ga, In, and La, and all halides. Overall, substitutions were performed for 12 systems. Fourth, following the substitution, the calculation of the phase diagram was conducted. Fifth, in the final step, battery-related features such as ionic conductivity, electrochemical stability window, and elastic constants were calculated for novel stable or metastable Li<sub>3</sub>MX<sub>6</sub> compositions.

Structure relaxation and total energy calculations were done using the density functional theory as implemented in the Vienna ab initio simulation package (VASP) [42,43] within the projector augmented-wave (PAW) method [44] and generalized gradient approximation (GGA) functional of Perdew, Burke, and Ernzerhof (PBE) [45]. The convergence of plane-wave cutoff energy and k-point mesh was tested for each structure and the highest values among all structures were selected for further calculations. The structural relaxation of substituted materials was done in several steps by tightening relaxation parameters (details are written in Supplementary Materials) [46–48]. After structure relaxation, phase diagrams for ternary Li - M - X systems were calculated [27]. The correction scheme described in [49] was applied to improve the accuracy of computed enthalpies of formation and phase stability predictions.

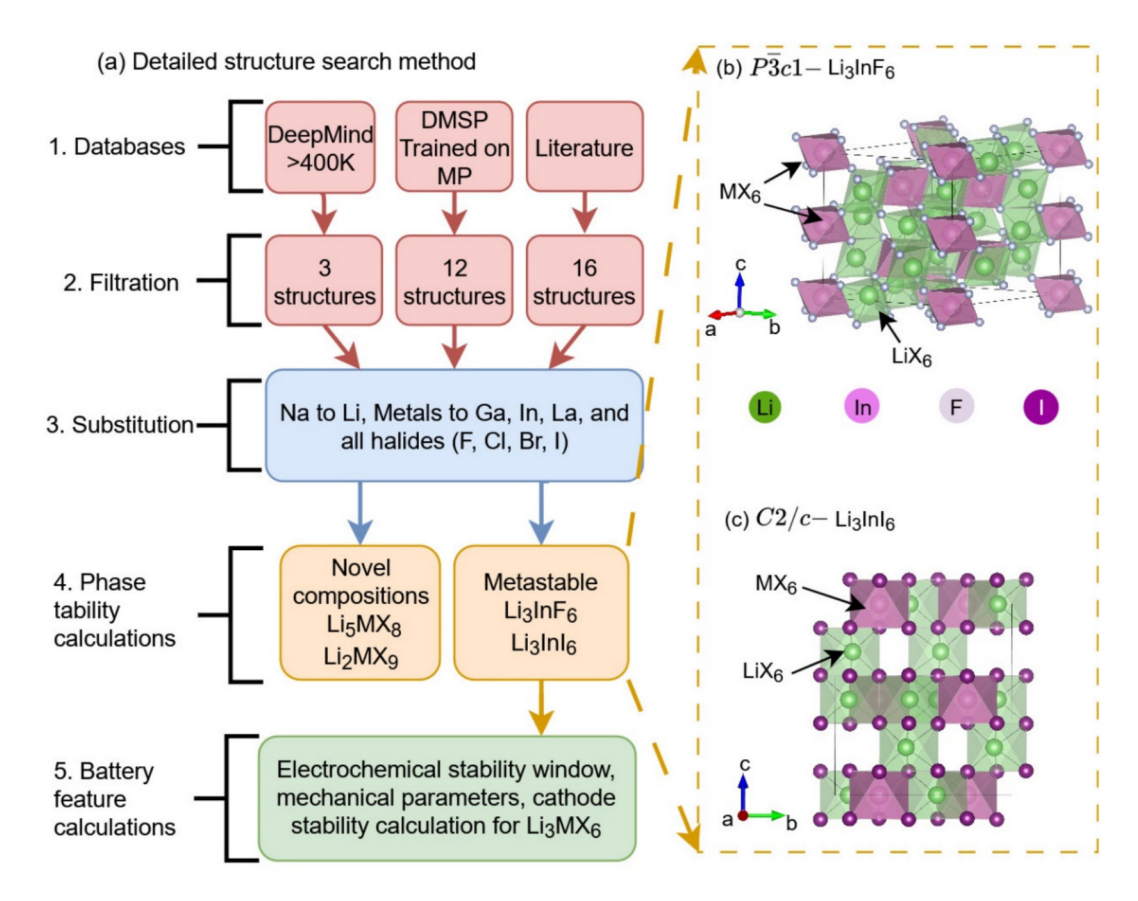


Fig. 1. Structure search method. (a) The flowchart of detailed structure search consisted of 1. Databases 2. Filtration 3. Substitution 4. Phase stability calculations 5. Battery related feature calculations. (b) The structure of predicted novel  $P3c1 - \text{Li}_3 \text{In} F6$ . (c) The structure of predicted.  $C2/c - \text{Li}_3 \text{In} I_6$ .

The supercell approach and the harmonic approximation, implemented through the Phonopy package [50,51], were utilized to compute vibrational frequencies. The dynamical stability of all structures, including both stable and metastable configurations, was confirmed by the absence of imaginary phonon frequencies.

Diffusion coefficients were calculated using mean square displacements (MSD) of Li<sup>+</sup> cations [52,53].

$$D = \left\{ \lim_{t \to \infty} d \left( \sum_{i=1}^{N} < |r_i(t) - r_i(0)|^2 > /N \right) / dt \right\} / 6$$
 (1)

where N – is number of the mobile atoms in the supercell, i – atomic number of mobile ion (Li),  $r_i(0)$ ,  $r_i(t)$  – radius vectors from the host center of mass to the i<sup>th</sup> atom at time 0 and t, respectively.

Ionic conductivity of lithium was calculated using the Nernst-Einstein formula [52].

$$\sigma = nq^2D/H_rk_BT \tag{2}$$

where n is the Li<sup>+</sup> ion density, q is the formal charge of the lithium ion (q = 1),  $k_B$  is Boltzmann constant, T is temperature and  $H_r$  is Haven ratio (assumed to be 1) [53].

To calculate ionic conductivity, more than 1 ns *ab initio* molecular dynamics simulation on a supercell is needed, which requires an enormous amount of computational time [52]. Therefore, the machine learned interatomic potential was constructed using MLIP-3 code [54]. Moment Tensor Potential (MTP) [55–57] of 20-th level was used for construction of potentials. The initial training set for the MLIPs was collected using AIMD and was improved within the Active Learning (AL) procedure [56]. We have performed validation tests for each MLIP. During calculation of ionic conductivities 2 % of Li vacancy was used, which may cause a little

overestimation, though the method is reliable and widely used for ionic conductivity calculation [16,53,58]. For more details about the training procedure, validation and the accuracy of the MLIPs see Figs. S1–S5 and Table S1 of the Supplementary Materials.

After construction of potentials, ionic conductivity was calculated using LAMMPS code [59,60] with NPT ensemble and Noose-Hoover thermostat [61,62]. Simulations were conducted for the supercells with lattice parameters no less than 30 Å and with 2 % vacancies on lithium sites. A timestep of 1 fs was used, and statistics were collected for 4 ns, with the preliminary equilibration of 1 ns at each temperature (300–500 K).

Activation energy  $E_{\rm a}$  of diffusion was calculated using the Arrhenius formula.

$$D = D_0 \times \exp(-E_a/k_BT) \tag{3}$$

The electrochemical stability of a solid-state electrolyte (SSE) material against decomposition of the SSE phase is commonly evaluated by calculating its Li-grand canonical phase diagram [63–65]. These diagrams were constructed using the pymatgen code [66]. Consistent with prior research, the electrostatic potential  $\phi$  was taken into account when determining the Li chemical potential  $\mu_{\rm Li}$ .

$$\mu_{\rm Li}(\phi) = \mu_{\rm Li}^0 - e\phi \tag{4}$$

where  $\mu_{\rm Li}$  is the chemical potential of Li metal, and  $\phi$  is the applied voltage referenced to Li metal. Interfacial stability between solid electrolytes and various cathode materials was also calculated using Li-grand canonical phase diagram as a function of Li chemical potential. The mechanical properties of novel materials were calculated regarding their symmetry, using elastic constants from VASP calculations [67,68]. The elastic constants were also used to estimate stability by Born elastic stability criterion. This criterion states

that for a mechanically stable compound, the relevant elastic tensor must be positive definite, that means all its eigenvalues must be positive [69].

#### 3. Results and discussion

#### 3.1. Detailed structure search

Among the 400,000 novel structures predicted by DeepMind [20], only three are included within the Li - M - X systems: LiGa<sub>2</sub>I<sub>9</sub> with space group  $P\bar{1}$ ,  $F\bar{4}3m-Li_4InF_7$  and  $I4_1/a-LiLaF_4$ . Each of these structures is classified as metastable and presents intriguing potential as ionic conductors due to their ability to provide intercalating pathways for Li-ion transport [20].

In addition to the structures previously described, the literature reports other experimentally synthesized or computationally predicted solid electrolytes. One notable example is Li<sub>3</sub>ErBr<sub>6</sub> [7], which crystallizes in the C2/m space group. Its stability has already been assessed for various systems, like Li<sub>3</sub>InCl<sub>6</sub> [11] and Li<sub>3</sub>InBr<sub>6</sub> [12]. To ensure the completeness of the structure type list, the Li<sub>3</sub>ErBr<sub>6</sub> structure with C2/m space group has also been included in our analysis. There are also a number of known and well-investigated structure types from literature [8], which are orthorhombic  $Pnma - \text{Li}_3 \text{YCl}_6$ ,  $Pna2_1 - \text{Li}_3 \text{AlF}_6$ ,  $Pna2_1 - \text{Li}_3 \text{YbCl}_6$ , trigonal  $P3m1 - \text{Li}_3 \text{ErCl}_6$ , monoclinic  $C2/c - \text{Li}_3 \text{AlF}_6$  (Table 1).

In recent publications, several structures with high ionic conductivity have gained attention, yet they remain underexplored for other compositions. Chen et al. from Microsoft utilized the

structure of  $Na_3YCl_6$  with an  $R\overline{3}$  space group to predict the metastable compound  $Na_2LiYCl_6$  [77]. Similarly, Zhu et al. computationally predicted novel metastable structures of  $Li_3Scl_6$  and  $Li_3Lal_6$ , exhibiting monoclinic symmetry with C2 and C2/c space groups [17]. In addition to the  $Li_3MX_6$  compositions, we included other non-stoichiometric compositions in our analysis due to their stable analogs in indium or gallium halide systems, such as  $LiGaCl_3$  [82] and  $LiGaCl_4$  [83]. Furthermore, the structure of  $Li_2Sc_{2/3}Cl_4$  was added to the list, because the compound  $Li_2In_{1/3}Sc_{2/3}Cl_4$  with high ionic conductivity has recently been synthesized, and it shows significant potential as a future solid-state electrolyte (SSE) [22].

Overall 31 structure types were filtered from DMSP, DeepMind and literature. These structures were further used for atom substitution and structure generation for 12 Li - M - X systems.

#### 3.2. Phase diagrams

For each of the 12 Li - M - X systems, we calculated the phase diagrams or convex hulls. In addition to the filtered structures, all known materials were incorporated into the stability diagrams. Our analysis confirmed the stability of all known double and ternary systems, validating the accuracy of our computational method. Furthermore, our calculations predicted that the known compounds  $\text{Li}_3 \text{InCl}_6$  and  $\text{Li}_3 \text{InBr}_6$  possess a C2/m space group, which matches existing literature [11,12]. Notably, even the 28.6 meV/ atom above hull energy of the metastable compound  $\text{Li}_3 \text{Lal}_6$  matched with the above hull energy mentioned in the literature [17].

**Table 1**Structure types of filtered materials. The composition is the taken from original structure. Also space group symbols with number in brackets, the source of database, Materials Project ID number, Experimentally observed, and Reference are listed.

#	Composition	Space group [number]	Source	MP ID	Experimentally observed	Reference
1	Li₃ErBr <sub>6</sub>	C2/m[12]	Literature	mp-1222492	Yes	[7,13]
2	Li <sub>3</sub> ErCl <sub>6</sub>	$P\bar{3}m1[164]$	Literature	mp-676361	Yes	[70]
3	Li <sub>3</sub> YbCl <sub>6</sub>	Pnma[62]	Literature	_	Yes	[70]
4	Li <sub>3</sub> ScI <sub>6</sub>	P2/m[10]	Literature	_	No	[17]
5	Li <sub>3</sub> ScI <sub>6</sub>	C2/c[15]	Literature	mp-1147621	No	[17]
6	Li <sub>3</sub> ScI <sub>6</sub>	C2[5]	Literature	mp-686004	No	[17]
7	Li <sub>3</sub> InCl <sub>6</sub>	C2[5]	Literature	mp-676109	No	[18]
8	Li <sub>3</sub> AlF <sub>6</sub>	C2/c[15]	Literature	mp-15254	Yes	[71]
9	Li <sub>3</sub> InCl6	Fm 3 m[255]	Literature	mp-1111288	No	[18]
10	Li <sub>3</sub> AlF6	Pna2 <sub>1</sub> [33]	Literature	mp-556020	Yes	[72]
11	Li <sub>3</sub> YbCl <sub>6</sub>	Pna2 <sub>1</sub> [33]	Literature	mp-637363	Yes	[73]
12	Li <sub>3</sub> ScF <sub>6</sub>	$P\bar{3}c1[165]$	DMSP	mp-560890	Yes	[74]
13	Na <sub>3</sub> InCl <sub>6</sub>	P3 1c[163]	DMSP	mp-23503	Yes	[75]
14	Na <sub>3</sub> InF <sub>6</sub>	$P2_{1}/c[14]$	DMSP	mp-1210420	No	[18]
15	Li <sub>3</sub> FeF <sub>6</sub>	$P\bar{3}1m[162]$	DMSP	mp-755087	No	[18]
16	Li₃FeF <sub>6</sub>	R 3 [148]	DMSP	mp-777459	No	[18]
17	Li <sub>3</sub> CrF <sub>6</sub>	P4n2[118]	DMSP	mp-769881	No	[18,76]
18	$Li_3VF_6$	P2 <sub>1</sub> [4]	DMSP	mp-767631	No	[18]
19	Li <sub>3</sub> VF <sub>6</sub>	<i>Cc</i> [9]	DMSP	mp-767671	No	[18]
20	Na <sub>3</sub> YCl <sub>6</sub>	R3 [148]	Literature	mp-675104	No	[77]
21	$\text{Li}_2\text{Sc}_{2/3}\text{Cl}_4$	Fd 3 m[227]	Literature	-	Yes	[22]
22	LiGa <sub>2</sub> I <sub>9</sub>	P 1 [2]	DeepMind	-	No	[20]
23	Li <sub>4</sub> InF <sub>7</sub>	F 4 3m[216]	DeepMind	-	No	[20]
24	LiLaF <sub>4</sub>	$I4_1/a[88]$	DeepMind	_	No	[20]
25	Li <sub>5</sub> CrCl <sub>8</sub>	Cmmm[65]	DMSP	mp-23361	Yes	[78]
26	$Rb_2In_3F_{11}$	$P2_1/m[11]$	DMSP	mp-554576	Yes	[79]
27	Rb <sub>2</sub> LaCl <sub>5</sub>	Pnma[62]	DMSP	mp-1209610	No	[80]
28	$Na_5Al_3F_{14}$	P4/mnc[128]	DMSP	mp-4752	Yes	[81]
29	LiGaCl₃	Pnma[62]	Literature	mp-29344	Yes	[82]
30	LiGaCl <sub>4</sub>	$P2_1/c[14]$	Literature	mp-28341	Yes	[83]
31	Li <sub>3</sub> InF <sub>6</sub>	$P2_1/m[11]$	Literature	_	Yes	[84,85]

#### 3.2.1. Li-In-F system

Magnus-Goldschmidt rule was used for description and search for the possible Li - M - X compositions [10,14]. According to the rule, if the ratio of cation to anion radius exceeds 0.732, the atoms tend to form  $MX_8$  cubes [10,14]. For example, Li - In - F system InF<sub>8</sub> cubes should be preferable, which is not aligned with experimental results [86], where InF<sub>6</sub> is more favorable and form the LiInF<sub>4</sub> [86] and  $\alpha - \text{Li}_3 \text{InF}_6$  [84,85] compositions. In our computed convex hull (Fig. 2),  $\alpha - \text{Li}_3 \text{In} F_6$  is classified as metastable, lying 16 meV/atom above the hull energy, a relatively small value that supports its classification as a metastable structure. In addition to the  $\alpha$ ,  $\beta$ , and  $\gamma$  phases have been synthesized. Our calculated phase diagram additionally reveals a novel structure with trigonal symmetry P3c1, which appears to be more stable, just 9 meV/ atom above the hull energy. This structure type is already known from  $P3c1 - Li_3ScF_6$  [74]. It features a hexagonal close-packed (hcp) anion sublattice with LiF<sub>6</sub> octahedra connected in a facesharing manner along the c-axis and in an edge-sharing manner within the a-b plane (Fig. 1).

#### 3.2.2. Li-In-I system

In the case of Li – In – I system, only LilnI<sub>4</sub> is known from the literature, and our calculations also confirm that LilnI<sub>4</sub> is stable (Fig. 3). Among the metastable Li<sub>3</sub>MX<sub>6</sub> compositions, the closest to hull structure type is Li<sub>3</sub>ScI<sub>6</sub> [17], which has a C2/c space group and lies just 4 meV/atom above the hull energy. Structures with C2/m and C2 symmetries are very similar. The Li<sub>3</sub>InI<sub>6</sub> structure with C2/c symmetry features InI<sub>6</sub> octahedra that are stacked in an AB sequence, similar to the arrangement in Li<sub>3</sub>ScI<sub>6</sub> [17]. In contrast, the stacking sequence for the C2/m structure is AA, while for the C2 structure, it is ABCD [17]. This variation in stacking can lower the total energy in certain materials, making them more favorable or stable compared to other Li<sub>3</sub>InI<sub>6</sub> structures. In addition to the Li<sub>3</sub>MX<sub>6</sub> compositions, we also discovered novel stable compositions, namely Li<sub>5</sub>InI<sub>8</sub> and LiIn<sub>2</sub>I<sub>9</sub>, within this sys-

tem. Details regarding these structure types will be provided in the next section.

#### 3.2.3. Novel compositions

Two stable structure types have been identified in the In and Ga systems:  $Cmmm - \text{Li}_5\text{MX}_8$  [78,87] and  $P\bar{1} - \text{LiM}_2\text{X}_9$  [20]. The compounds  $\text{Li}_5\text{InCl}_8$ ,  $\text{Li}_5\text{InBr}_8$  and  $\text{Li}_5\text{InI}_8$  are stable and lie on the convex hull. In contrast,  $\text{Li}_5\text{GaBr}_8$  and  $\text{Li}_5\text{GaI}_8$  are metastable, with energies less than 18 meV/atom above the hull. The  $\text{Li}_5\text{MX}_8$  structure features a face-centered cubic (fcc) anionic framework with orthorhombic symmetry, where the M and Li atoms form octahedra units with anions (Fig. 4). These  $\text{MX}_6$  form isolated, edgesharing, or corner-sharing units with  $\text{LiX}_6$  octahedra and form layered structures [88], which may enhance the ionic conductivity in this composition [87,89].

The next structure type,  $LiM_2X_9$ , with triclinic P1 symmetry, was predicted by DeepMind in the Li-Ga-I system [20]. Interestingly, this composition is also thermodynamically stable in the M=In and X=Cl, Br, and I systems. An additional structure search for fixed composition was conducted using USPEX [24,25,27] to ensure structural stability. The resulting  $P1-LiM_2X_9$  structure is more favorable than the  $P\bar{1}-LiM_2X_9$  structure from DeepMind. In the predicted structure, M atoms form tetrahedral  $MX_4$  and octahedral  $MX_6$  units (Fig. 4). The  $MX_4$  units share edges with Li atoms situated between them, while the  $MX_6$  units share two edges with nearby octahedra.

#### 3.3. Phonon calculation

The dynamical stability calculations for the  $P3\,c1-Li_3InF_6$  and  $C2/c-Li_3InI_6$  structures did not reveal any imaginary frequencies, confirming their dynamical stability (Fig. 5a and b). Similarly, the non-stoichiometric structures Li<sub>5</sub>InCl<sub>8</sub>, Li<sub>5</sub>InBr<sub>8</sub>, Li<sub>5</sub>InI<sub>8</sub>, LiIn<sub>2</sub>Cl<sub>9</sub>, LiIn<sub>2</sub>Br<sub>9</sub>, and LiIn<sub>2</sub>I<sub>9</sub> also showed no imaginary frequencies (Fig. S7).

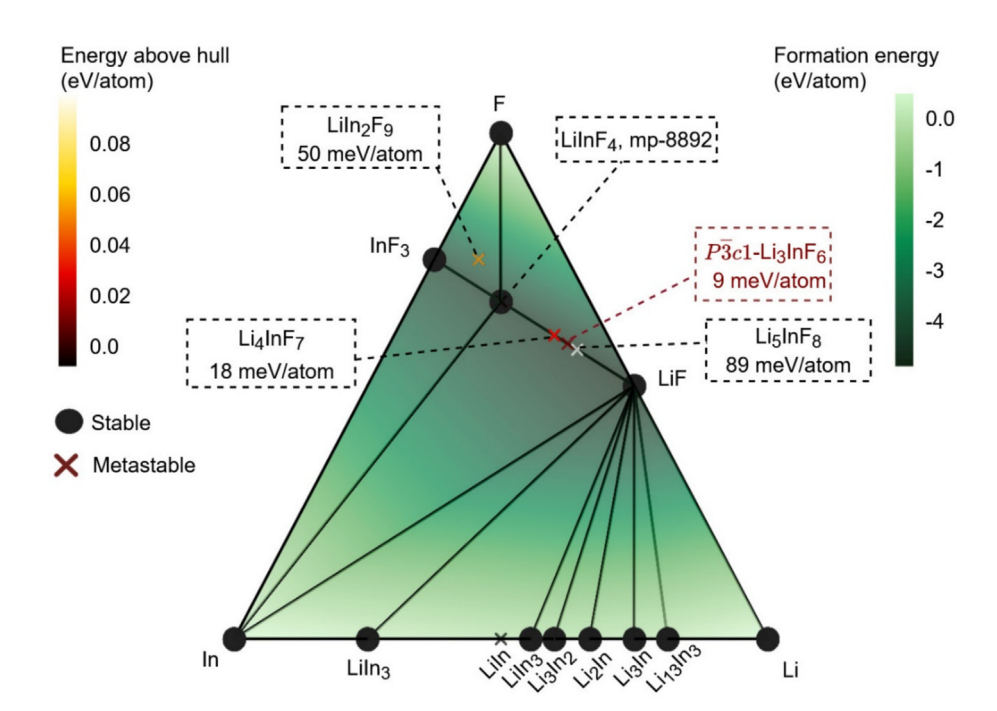


Fig. 2. Phase diagram of Li – In – F ternary system. Stable materials are marked with black circles, metastable structures with crosses, the color of which varies according to above hull energy. Only stable, metastable and novel compositions are shown the figure for simplicity.

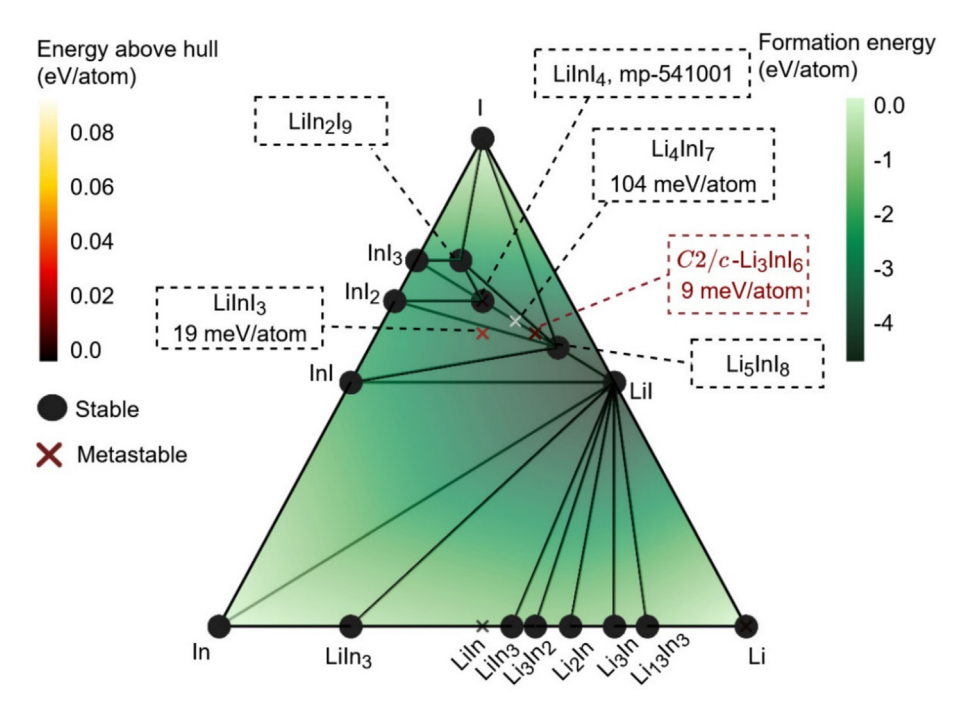


Fig. 3. Phase diagram of Li - In - I ternary system. Stable materials are marked with black circles, metastable structures with crosses, the color of which color varies according to above hull energy. Only stable, metastable and novel compositions are shown the figure for simplicity.

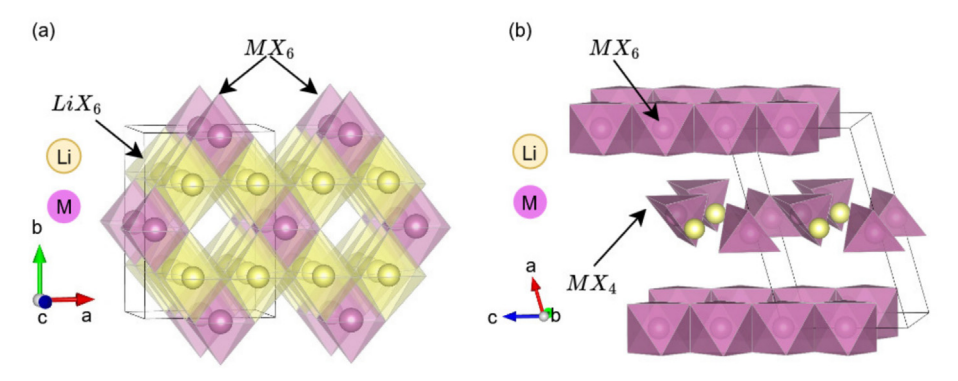


Fig. 4. Crystal structures of novel compositions. (a)  $Cmmm - Li_5MX_8$ , (b)  $P1 - LiM_2X_9$ .

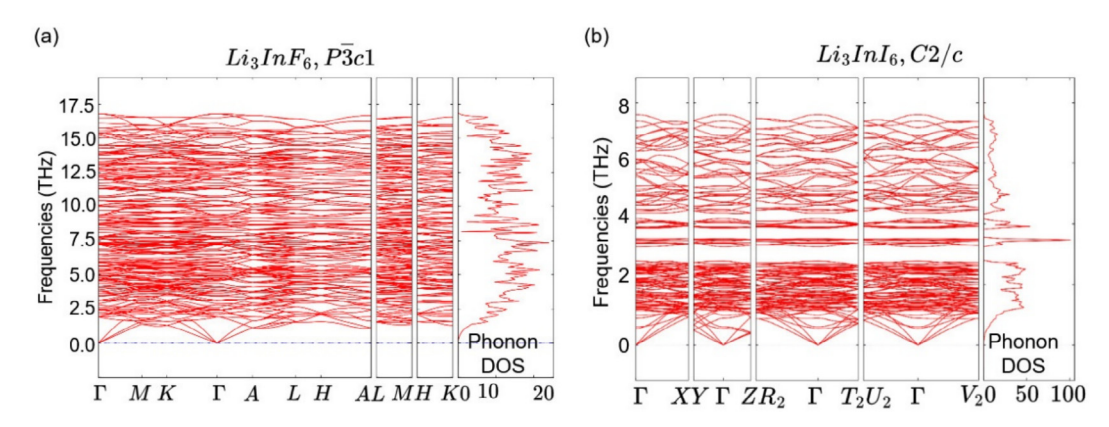


Fig. 5. Phonon dispersion and phonon density of states of novel predicted materials. (a)  $P\overline{3}c1 - Li_3InF_6$ , (b)  $C2/c - Li_3InI_6$ .

#### 3.4. Ionic conduction and diffusion coefficients

The lithium ion conductivities obtained from molecular dynamics simulations with MLIP are 0.55 mS/cm for  $P\bar{3}c1 - Li_3InF_6$  and 2.18 mS/cm for  $C2/c - Li_3InI_6$  at 300 K. To be considered a prospective solid-state electrolyte (SSE), a material should exhibit an ionic conductivity of approximately 1 mS/cm. The newly identified  $P\bar{3}c1 - Li_3InF_6$  meets this requirement and even surpasses  $Li_3ScF_6$  (0.28 mS/cm) [74]. The  $C2/c - Li_3InI_6$  phase outperforms all of its analogues, including  $Li_3YCI_6$ ,  $Li_3YBr_6$ ,  $Li_3LaI_6$ , and  $Li_3InCI_6$  (Table 2). Although sulfide-based SSEs generally possess higher ionic conductivities, they have a narrower electrochemical stability window (Table 2).

The Arrhenius plots for these  $\mathrm{Li_3MX_6}$  materials are shown in Fig. 6(a and b). The activation energies calculated from the Arrhenius plots are 259 meV for  $P\overline{3}c1-\mathrm{Li_3InF_6}$  and 268 meV for  $C2/c-\mathrm{Li_3InI_6}$ . More details for activation energies, ionic conductivities and diffusion coefficients are shown in the Tables S4–S6 in the Supplementary Materials.

These activation barriers are lower compared to those of  $P\bar{3}c1 - \text{Li}_3\text{SCCl}_6$  at 310 meV [74],  $\text{Li}_3\text{YCl}_6$  at 400 meV [7], and  $C2/c - \text{Li}_3\text{Lal}_6$  [17], along with numerous other halide solid electrolytes [2,5,10]. Some researchers have shown that in general, monoclinic halide SSEs with cubic anion sublattices exhibit higher ionic conductivities, with the general trend being  $\sigma_{\text{monoclinic}} > \sigma_{\text{orthorhombic}} > \sigma_{\text{trigonal}}$  [14]. In contrast,  $\text{Li}_3\text{InF}_6$ , which features a hexagonal anionic sublattice with  $P\bar{3}c1$  symmetry, demonstrates a lower activation barrier and comparable ionic conductivity. This finding suggests that hexagonal anionic sublattices should also be considered as potential candidates for future research.

Additionally, we calculated the activation energies along the a, b, and c directions for  $\text{Li}_3\text{InF}_6$  and  $\text{Li}_3\text{InI}_6$  using Arrhenius fitting; the results are presented in Table S4.

As illustrated in Fig. 6 and Table S4, three-dimensional lithium diffusion channels exist with very low activation barriers. All other halide high-ionic conductors lack three-dimensional ionic paths, indicating that  $P^{-3}c1 - \text{Li}_3 \text{InF}_6$  is a promising new high-ionic halide conductor. In the case of  $C2/c - \text{Li}_3 \text{InI}_6$ , the activation barriers differ, with higher values observed in the a and b directions, similar to other  $C2/m - \text{Li}_3 \text{MX}_6$  materials [11]. The lithium ion migration paths in this monoclinic structure include three-dimensional cross-layer pathways (Fig. 6c and d) [7]. However, in all directions, the barrier values are not so high and enable homogeneous diffusion channels (Table S4).

The AIMD with MLIP simulation also reveals the temperature stability of these materials until 600 K (Fig. S10), which can be a guide for experimental groups for synthesis. The volume change during heating and cooling show that starting from 600 K the

structures undergoes volume distortions, which identify the instability (Fig. S10).

#### 3.5. Electrochemical stability

A wide band gap is a crucial characteristic of solid-state electrolytes, because it prevents the shortage of electrodes. Additionally, band gap enables the determination of the electrochemical stability window. The new compound  $P\bar{3}c1-\text{Li}_3\text{InF}_6$  exhibits a band gap of 5 eV, while  $\text{Li}_3\text{InI}_6$  has a band gap of 2.5 eV. However, these band gaps represent only the upper limits of the electrochemical stability windows. To obtain more accurate stability windows, we employed grand canonical phase diagrams.

As shown in Fig. 7(a),  $P\bar{3}c1 - \text{Li}_3 \text{lnF}_6$  has a wide stability window of approximately 4 V, which is consistent with other fluoride solid-state electrolytes [74]. In contrast, the stability window for  $C2/c - \text{Li}_3 \text{lnI}_6$  is 0.7 eV (Fig. 7b), aligning with the stability windows observed for iodides [9].

The stability of these materials against common cathodes such as  $LiCoO_2$ ,  $LiFePO_4$ , and  $LiMnO_2$  was assessed through reaction energy calculations using the grand canonical phase diagram across various voltages (Figs. S9 and S10). It is evident that all reaction energies are small compared to sulfides and are close to known halide solid-state electrolytes [4,17], confirming their stability against the selected cathodes. The combination of high ionic conductivity and stability against both anodes and cathodes makes  $P \ 3c1 - Li_3 lnF_6$  and  $C2/c - Li_3 lnI_6$  promising candidates for experimental exploration and application in all-solid-state electrolytes.

#### 3.6. Mechanical parameters

The calculated elastic constants are presented in Table S7. The analysis of elastic stability criteria confirmed the stability of  $P\bar{3}c1-Li_3InF_6$ ,  $C2/c-Li_3InI_6$ , and the novel compositions  $Li_5InCI_8$ ,  $Li_5InBr_8$ ,  $Li_5InI_8$ ,  $LiI_02CI_9$ ,  $LiI_02Br_9$ , and  $LiI_02I_9$ . Monroe et al. proposed that if the shear modulus of an SSE exceeds twice that of lithium (4.8 GPa at room temperature), lithium dendrites will not form.  $Li_3InF_6$  exhibits a shear modulus of 28.08 GPa and a hardness of 5.5 GPa, making it a promising candidate for an SSE. All other mechanically stable materials also meet this criterion (Table S7) [90].

#### 4. Conclusions

In this study, we conducted a detailed structural search for  $\text{Li}_3\text{MX}_6$  compositions, where M represents In, Ga, or La, and X includes F, Cl, Br, and I. This comprehensive search involved DMSP calculations and the compilation of novel structures from Deep-Mind data and existing literature. As  $\underline{a}$  result, we identified two metastable structures:  $\text{Li}_3\text{InF}_6$  with P3c1 symmetry and  $\text{Li}_3\text{InI}_6$ 

**Table 2**The important parameters of novel and known materials for battery applications.

Composition	Ionic conductivity (mS/cm)	$E_{\rm a}$ (meV)	Electrochemical stability window (V)	$E_{\rm g}$ (eV)	Ref.
Li <sub>3</sub> InF <sub>6</sub>	0.55	259	4	5	this article
Li <sub>3</sub> InI <sub>6</sub>	2.18	268	0.7	2.5	this article
Li <sub>3</sub> ScF <sub>6</sub>	0.28	310	5	6.7	[74]
Li <sub>3</sub> YCl <sub>6</sub>	0.51	400	3.2	6.1	[7]
Li <sub>3</sub> YBr <sub>6</sub>	1.7	400	2.2	5.1	[7]
Li <sub>3</sub> LaI <sub>6</sub>	0.99	298	2	3	[17]
Li <sub>3</sub> InCl <sub>6</sub>	1.49	325	1.5	5	[9]
Li <sub>10</sub> GeP <sub>2</sub> S <sub>12</sub>	9	210	0.4	3.6	[4,52]
Li <sub>6</sub> PS <sub>5</sub> Cl	1.3	250	2	2.7	[4,52]

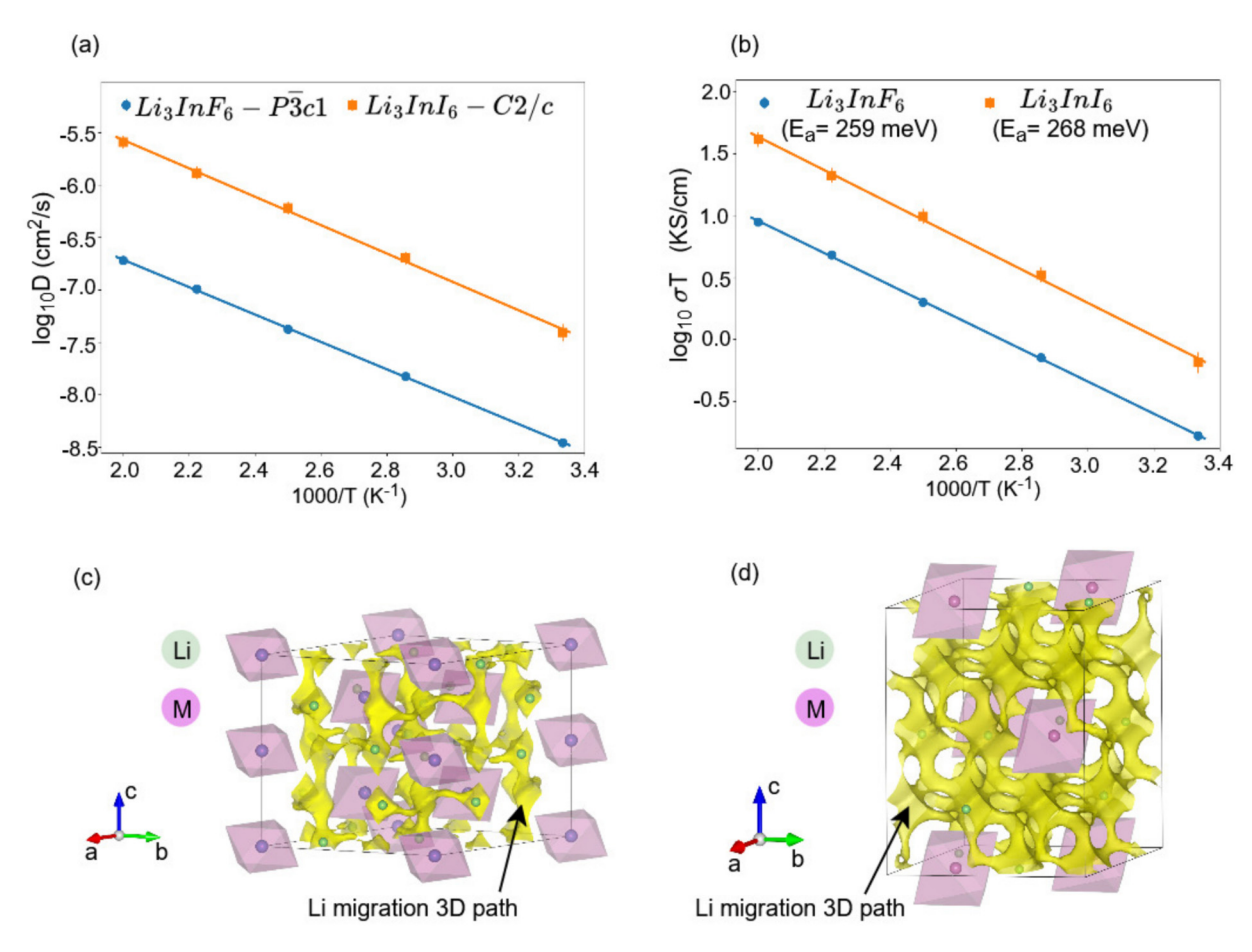


Fig. 6. Ionic conductivities and diffusion paths for novel materials. (a) Diffusion coefficient and (b) ionic conduction as functions of temperatures, (c and d) are crystal structure and Li-ion migration paths plotted with Li-ion density isosurface (with value  $0.6/\text{Å}^3$ ) for Li<sub>3</sub>InF<sub>6</sub> and Li<sub>3</sub>InI<sub>6</sub> respectively.

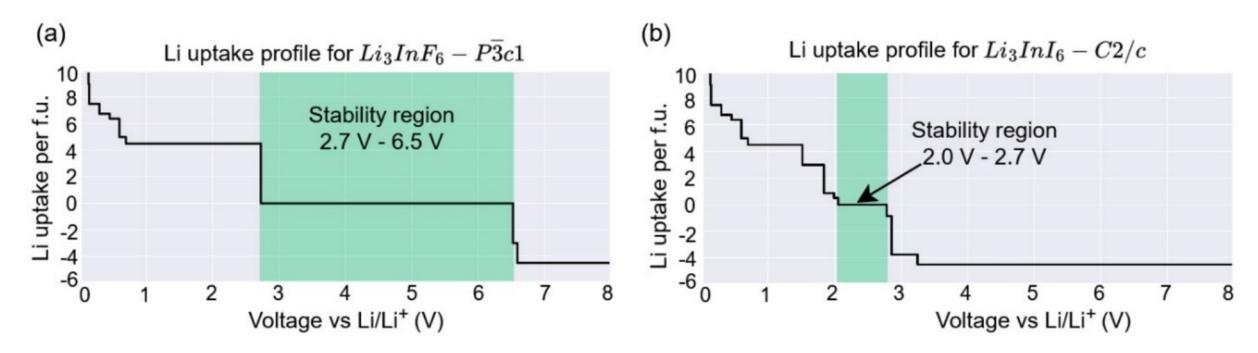


Fig. 7. Electrochemical stability windows, where stability against Li uptake and voltages are shown. The green background show the range of stability ranges of (a) Li<sub>3</sub>InF<sub>6</sub> and (b) Li<sub>3</sub>InI<sub>6</sub> materials.

with C2/c symmetry. We also predicted the stable structures with new compositions of  $Li_5InCl_8$ ,  $Li_5InBr_8$ ,  $Li_5Inl_8$ ,  $LiIn_2Cl_9$ ,  $LiIn_2Br_9$  and  $LiIn_2I_9$ . The stability of the new  $Li_3MX_6$  compound was further confirmed through phonon calculations, which revealed no imaginary frequencies, as well as through elastic stability criteria.

Calculations of Li-ion conduction using ab initio molecular dynamics (AIMD) and machine learning interatomic potentials (MLIP) demonstrated that the novel compounds  $P\bar{3}c1-\text{Li}_3\text{InF}_6$  and  $C2/c-\text{Li}_3\text{InI}_6$  exhibit high ionic conductivities of 0.55 and 2.18 mS/cm at 300 K, respectively. Ionic conduction path analyses using MD revealed a three-dimensional network, with low activation barriers 259 meV for  $P\bar{3}c1-\text{Li}_3\text{InF}_6$  and 268 meV for  $C2/c-\text{Li}_3\text{InI}_6$ .

The electrochemical stability windows for  $\text{Li}_3\text{InI}_6$  and  $\text{Li}_3\text{InF}_6$  are 0.7 and 4 V, respectively. Taken together, these materials emerge as promising solid electrolytes for next-generation all-solid-state batteries. In future work, we will extend our investigation to the full range of newly predicted compositions and experimentally verify the stability of novel materials.

#### **CRediT authorship contribution statement**

Olgert L. Dallakyan: Methodology, Investigation. Alexey P. Maltsev: Methodology, Investigation. Ilya V. Chepkasov: Investigation. Misha A. Aghamalyan: Investigation. Areg A. Hunanyan: Investigation. Nane Z. Petrosyan: Investigation. Mikayel S. Chobanyan: Investigation. Mikayel T. Sahakyan: Investigation. Luiza

**G. Khachatryan:** Investigation. **Artem R. Oganov:** Writing – review & editing, Formal analysis. **Hayk A. Zakaryan:** Writing – original draft, Supervision, Methodology, Investigation, Conceptualization.

#### **Declaration of competing interest**

The authors declare that they have no known competing financial interests or personal relationships that could have appeared to influence the work reported in this paper.

#### **Acknowledgments**

The work was supported by the Higher Education and Science Committee of Armenia in the frames of the research projects 20TTSG-2F010, 23AA-2F033 and ANSEF (EN-matsc-2660) grant. Convex hull calculations were done on the Oracle HPC clouds provided by the Oracle for Research grant (16576595). The USPEX calculations were performed on the Armenian National Supercomputing Center (ANSCC). MLIP training and ionic conductivity calculations were performed with the support of the Russian Science Foundation (RSF) grant no. 19-72-30043, and using the resources of the Center for Information and Computing of the Research Center for Information and Computational Technologies at Novosibirsk State University.

#### Appendix A. Supplementary material

Supplementary data to this article can be found online at https://doi.org/10.1016/j.jechem.2025.08.047.

#### References

- [1] M. Fichtner, K. Edström, E. Ayerbe, M. Berecibar, A. Bhowmik, I.E. Castelli, S. Clark, R. Dominko, M. Erakca, A.A. Franco, A. Grimaud, B. Horstmann, A. Latz, H. Lorrmann, M. Meeus, R. Narayan, F. Pammer, J. Ruhland, H. Stein, T. Vegge, M. Weil, Adv. Energy Mater. 2102904 (2021).
- [2] A. Manthiram, X. Yu, S. Wang, Nat. Rev. Mater. 2 (2017) 1–16.
- [3] Y. Wang, W.D. Richards, S.P. Ong, L.J. Miara, J.C. Kim, Y. Mo, G. Ceder, Nat. Mater. 14 (2015) 1026–1031.
- [4] W. Zhao, J. Yi, P. He, H. Zhou, Electrochem. Energy Rev. 2 (2019) 574-605.
- [5] X. Nie, J. Hu, C. Li, Interdiscip. Mater. 2 (2023) 365–389.
- [6] D.C. Ginnings, T.E. Phipps, J. Am. Chem. Soc. 52 (1930) 1340–1345.
- [7] T. Asano, A. Sakai, S. Ouchi, M. Sakaida, A. Miyazaki, S. Hasegawa, Adv. Mater. 30 (2018) 1–7.
- [8] X. Li, J. Liang, X. Yang, K.R. Adair, C. Wang, F. Zhao, X. Sun, Energy Environ. Sci. 13 (2020) 1429–1461.
- [9] K. Kim, D. Park, H.G. Jung, K.Y. Chung, J.H. Shim, B.C. Wood, S. Yu, Chem. Mater. 33 (2021) 3669–3677.
- [10] J. Liang, X. Li, K.R. Adair, X. Sun, Acc. Chem. Res. 54 (2021) 1023–1033.
- [11] X. Li, J. Liang, J. Luo, M. Norouzi Banis, C. Wang, W. Li, S. Deng, C. Yu, F. Zhao, Y. Hu, T.K. Sham, L. Zhang, S. Zhao, S. Lu, H. Huang, R. Li, K.R. Adair, X. Sun, Energy Environ. Sci. 12 (2019) 2665–2671.
- [12] Y. Tomita, K. Yamada, H. Ohki, T. Okuda, Zeitschrift Für Naturforsch. A 53 (1998) 4–10.
- [13] S. Wang, Q. Bai, A.M. Nolan, Y. Liu, S. Gong, Q. Sun, Y. Mo, Angew. Chemie Int. Ed. 58 (2019) 8039–8043.
- [14] C. Wang, J. Liang, J.T. Kim, X. Sun, Sci. Adv. 8 (2022) 1-14.
- [15] J. Park, D. Han, H. Kwak, Y. Han, Y.J. Choi, K.W. Nam, Y.S. Jung, Chem. Eng. J. 425 (2021) 130630.
- [16] D. Park, H. Park, Y. Lee, S.O. Kim, H.G. Jung, K.Y. Chung, J.H. Shim, S. Yu, ACS Appl. Mater. Interfaces 12 (2020) 34806–34814.
- [17] Z. Xu, X. Chen, K. Liu, R. Chen, X. Zeng, H. Zhu, Chem. Mater. 31 (2019) 7425–7433.
- [18] A. Jain, S.P. Ong, G. Hautier, W. Chen, W.D. Richards, S. Dacek, S. Cholia, D. Gunter, D. Skinner, G. Ceder, K.A. Persson, APL Mater. 1 (2013).
- [19] S. Kirklin, J.E. Saal, B. Meredig, A. Thompson, J.W. Doak, M. Aykol, S. Rühl, C. Wolverton, Npj Comput. Mater. 1 (2015).
- [20] A. Merchant, S. Batzner, S.S. Schoenholz, M. Aykol, G. Cheon, E.D. Cubuk, Nature 624 (2023) 80–85.
- [21] F. Hussain, J. Zhu, H. Xia, Y. Zhao, W. Xia, J. Phys. Chem. C 126 (2022) 13105–13113
- [22] L. Zhou, C.Y. Kwok, A. Shyamsunder, Q. Zhang, X. Wu, L.F. Nazar, Energy Environ. Sci. 13 (2020) 2056–2063.

- [23] Q. Wang, Y. Zhou, X. Wang, H. Guo, S. Gong, Z. Yao, F. Wu, J. Wang, S. Ganapathy, X. Bai, B. Li, C. Zhao, J. Janek, M. Wagemaker, Nat. Commun. 15 (2024) 1–10.
- [24] A.R. Oganov, C.W. Glass, J. Chem. Phys. 124 (2006) 244704.
- [25] A.R. Oganov, M. Valle, J. Chem. Phys. 130 (2009) 104504.
- [26] A.O. Lyakhov, A.R. Oganov, M. Valle, Comput. Phys. Commun. 181 (2010) 1623–1632.
- [27] A.R. Oganov, C.J. Pickard, Q. Zhu, R.J. Needs, Nat. Rev. Mater. 4 (2019) 331-348.
- [28] A.V. Iosimovska, A.P. Maltsev, I.V. Chepkasov, A.R. Oganov, Appl. Phys. Lett. 124 (2024) 163904.
- [29] A.P. Maltsev, I.V. Chepkasov, A.R. Oganov, Mater. Today Energy 39 (2024) 101467.
- [30] C.J. Pickard, R.J. Needs, J. Phys. Condens. Matter 23 (2011) 53201.
- [31] A. Hunanyan, N. Petrosyan, H. Zakaryan, Appl. Surf. Sci. 672 (2024) 160814.
- [32] A. Hunanyan, V.M. Aroutiounian, H. Zakaryan, J. Phys. Chem. C 126 (n.d.) 4647–4654.
- [33] A. Kvashnin, C. Tantardini, H. Zakaryan, Y. Kvashnina, A. Oganov, Chem. Mater. 32 (n.d.) 7028–7035.
- [34] A.G. Kvashnin, H.A. Zakaryan, C. Zhao, Y. Duan, Y.A. Kvashnina, C. Xie, H. Dong, A.R. Oganov, J. Phys. Chem. Lett. 9 (2018) 3470–3477.
- [35] H.A. Zakaryan, A.G. Kvashnin, A.R. Oganov, Sci. Rep. 7 (2017) 10357.
- [36] E.V. Sukhanova, A.G. Kvashnin, L.A. Bereznikova, H.A. Zakaryan, M.A. Aghamalyan, D.G. Kvashnin, Z.I. Popov, Appl. Surf. Sci. 589 (2022) 152971.
- [37] I.V. Chepkasov, E.V. Sukhanova, A.G. Kvashnin, H.A. Zakaryan, M.A. Aghamalyan, Y.S. Mamasakhlisov, A.M. Manakhov, Z.I. Popov, D.G. Kvashnin, Nanomaterials 12 (2022).
- [38] C. Xie, Q. Zhang, H.A. Zakaryan, H. Wan, N. Liu, A.G. Kvashnin, A.R. Oganov, J. Appl. Phys. 125 (2019) 205109.
- [39] G. Hautier, C. Fischer, V. Ehrlacher, A. Jain, G. Ceder, Inorg. Chem. 50 (2011) 656–663.
- [40] P. Hohenberg, W. Kohn, Phys. Rev. 136 (1964) B864-B871.
- [41], Phys. Rev. 140 (1965) A1133-A1138.
- [42] G. Kresse, J. Hafner, Phys. Rev. B 49 (1994) 14251-14269.
- [43] G. Kresse, J. Furthmüller, Phys. Rev. B 54 (1996) 11169-11186.
- [44] D. Joubert, Phys. Rev. B Condens. Matter Mater. Phys. 59 (1999) 1758-1775.
- [45] J.P. Perdew, K. Burke, M. Ernzerhof, Phys. Rev. Lett. 77 (1996) 3865–3868.
- [46] M.A. Aghamalyan, V.M. Aroutiounian, E.S. Mamasakhlisov, E.V. Sukhanova, A. G. Kvashnin, Z.I. Popov, A.A. Zakaryan, J. Contemp. Phys. (Armenian Acad. Sci. 57 (2022) 170–173.
- [47] M.A. Aghamalyan, A.A. Hunanyan, V.M. Aroutiounian, M.S. Aleksanyan, A.G. Sayunts, H.A. Zakaryan, J. Contemp. Phys. (Armen. Acad. Sci.) 55 (2020) 235–239
- [48] C. Tantardini, H.A. Zakaryan, Z. Han, T. Altalhi, S.V. Levchenko, A.G. Kvashnin, I. Yakobson, J. Comput. Sci. 82 (2024) 102402.
- [49] A. Wang, R. Kingsbury, M. McDermott, M. Horton, A. Jain, S.P. Ong, S. Dwaraknath, K.A. Persson, Sci. Rep. 11 (2021).
- [50] A. Togo, L. Chaput, T. Tadano, I. Tanaka, J. Phys. Condens. Matter 35 (2023) 353001.
- [51] A. Togo, J. Phys. Soc. Jpn. 92 (2023) 12001.
- [52] L. Xia, H. Liu, Y. Pei, Nanoscale (2024) 15481–15501.
- [53] A.P. Maltsev, I.V. Chepkasov, A.R. Oganov, ACS Appl. Mater. \& Interfaces 15 (2023) 42511–42519.
- [54] I.S. Novikov, K. Gubaev, E.V. Podryabinkin, A.V. Shapeev, Mach. Learn.: Sci. Technol. 2 (2021) 025002.
- [55] A.V. Shapeev, Multiscale Model. & Simul. 14 (2016) 1153-1173.
- [56] E.V. Podryabinkin, A.V. Shapeev, Comput. Mater. Sci 140 (2017) 171–180.
- [57] E.V. Podryabinkin, E.V. Tikhonov, A.V. Shapeev, A.R. Oganov, Phys. Rev. B 99 (2019) 1-7.
- [58] A.K. Sagotra, D. Chu, C. Cazorla, Phys. Rev. Mater. 3 (2019) 35405.
- [59] S. Plimpton, J. Comput. Phys. 117 (1995) 1–19.
- [60] A.P. Thompson, H.M. Aktulga, R. Berger, D.S. Bolintineanu, W.M. Brown, P.S. Crozier, P.J. in't Veld, A. Kohlmeyer, S.G. Moore, T.D. Nguyen, et al., Comput. Phys. Commun. 271 (2022) 108171.
- [61] W.G. Hoover, Phys. Rev. A 34 (1986) 2499.
- [62] D.J. Evans, B.L. Holian, J. Chem. Phys. 83 (1985) 4069–4074.
- [63] Y. Zhu, X. He, Y. Mo, ACS Appl. Mater. Interfaces 7 (2015) 23685–23693.
- [64] T. Binninger, A. Marcolongo, M. Mottet, V. Weber, T. Laino, J. Mater. Chem. A 8 (2020) 1347–1359.
- [65] W.D. Richards, L.J. Miara, Y. Wang, J.C. Kim, G. Ceder, Chem. Mater. 28 (2016) 266–273.
- [66] S.P. Ong, W.D. Richards, A. Jain, G. Hautier, M. Kocher, S. Cholia, D. Gunter, V.L. Chevrier, K.A. Persson, G. Ceder, Comput. Mater. Sci 68 (2013) 314–319.
- [67] Z. Wu, E. Zhao, H. Xiang, X. Hao, X. Liu, J. Meng, Phys. Rev. B 76 (2007) 54115.
- [68] Z. Deng, Z. Wang, I.-H. Chu, J. Luo, S.P. Ong, J. Electrochem. Soc. 163 (2015) A67.
- [69] F. Mouhat, F.-X. Coudert, Phys. Rev. B 90 (2014) 224104.
- [70] K.H. Park, K. Kaup, A. Assoud, Q. Zhang, X. Wu, L.F. Nazar, ACS Energy Lett. (2020) 533–539.
- [71] M. Feinauer, H. Euchner, M. Fichtner, M. Anji Reddy, ACS Appl. Energy Mater. 2 (2019) 7196–7203.
- [72] T. Esaka, R. Okuyama, H. Iwahara, Solid State Ion. 34 (1989) 201–205.
- [73] S.Y. Kim, K. Kaup, K.H. Park, A. Assoud, L. Zhou, J. Liu, X. Wu, L.F. Nazar, ACS Mater. Lett. 3 (2021) 930–938.
- [74] J. Liu, S. Wang, Y. Qie, Q. Sun, Mater. Today Energy 21 (2021) 100719.
- [75] T. Zhao, M.A. Kraft, W.G. Zeier, Inorg. Chem. 62 (2023) 11737–11745.
- [76] A.K. Tyagi, J. Köhler, Mater. Res. Bull. 35 (2000) 135–141.

- [77] C. Chen, D.T. Nguyen, S.J. Lee, N.A. Baker, A.S. Karakoti, L. Lauw, C. Owen, K.T. Mueller, B.A. Bilodeau, V. Murugesan, M. Troyer, J. Am. Chem. Soc. 146 (2024) 20009-20018.
- [78] H.D. Lutz, P. Kuske, A. Pfitzner, H.-J. Steiner, Zeitschrift Für Naturforsch. B 47 (1992) 1687-1692.
- [79] J.-C. Champarnaud-Mesjard, B. Frit, Acta Crystallogr. Sect. B 34 (1978) 736-741.
- [80] G. Shwetha, G. Vaitheeswaran, V. Kanchana, A.I.P. Conf, Proc 1665 (2015) 120026.
- [81] P. Rocquet, M. Couzi, A. Tressaud, J.P. Chaminade, C. Hauw, J. Phys. C Solid State Phys. 18 (1985) 6555.
- [82] W. Hönle, G. Miller, A. Simon, J. Solid State Chem. 75 (1988) 147-155.

- [83] W. Hönle, B. Hettich, A. Simon, Zeitschrift Für Naturforsch. B 42 (1987) 248-250
- [84] M. Hamadène, F. Balegroune, A. Guehria-Laïdoudi, J. Grannec, J. Ravez, J. Chem. Crystallogr. 36 (2006) 1-5.
- [85] M. Hamadène, J. Ravez, J. Grannec, A. Laïdoudi-Guehria, Mater. Lett. 27 (1996) 33-39.
- [86] P. Gravereau, J.P. Chaminade, T. Gaewdang, J. Grannec, M. Pouchard, P. Hagenmuller, Acta Crystallogr. Sect. C 48 (1992) 769–771.
- [87] Q. Yang, J. Xu, Y. Wang, X. Fu, R. Xiao, H. Li, (2024).
- [88] Z. Li, H. Dong, B. Zhang, ACS Appl. Mater. Interfaces 15 (2023) 42481–42489. [89] Y. Liu, S. Wang, A.M. Nolan, C. Ling, Y. Mo, Adv. Energy Mater. 10 (2020) 1–11.
- [90] C. Monroe, J. Newman, J. Electrochem. Soc. 152 (2005) A396.